Identification and Characterization of a Au(III) Reductase from *Erwinia* sp. IMH

Liying Wang,[∥] Li Yan,[∥] Li Ye, Jinfeng Chen, Yanwei Li, Qingzhu Zhang, and Chuanyong Jing*

Cite This: *JACS Au* 2022, 2, 1435−1442

Read Online

ACCESS | ▬ Metrics & More | ▬ Article Recommendations | ▬ Supporting Information

ABSTRACT: Microorganisms contribute to the formation of secondary gold (Au) deposits through enzymatic reduction of Au(III) to Au(0). However, the enzyme that catalyzes the reduction of Au(III) remains enigmatic. Here, we identified and characterized a previously unknown Au reductase (GolR) in the cytoplasm of *Erwinia* sp. IMH. The expression of *golR* was strongly up-regulated in response to increasing Au(III) concentrations and exposure time. Mutant with in-frame deletion of *golR* was incapable of reducing Au(III), and the capability was rescued by reintroducing wild-type *golR* into the mutant strain. The Au(III) reduction was determined to occur in the cytoplasmic space by comparing the TEM images of the wild-type, mutant, and complemented strains. In vitro assays of the purified GolR protein confirmed its ability to reduce Au(III) to Au nanoparticles. Molecular dynamic simulations demonstrated that the hydrophobic cavity of GolR may selectively bind $AuCl_2(OH)_2^-$, the predominant auric chloride species at neutral pH. Density functional theory calculations revealed that $AuCl_2(OH)_2^-$ may be coordinated at the Fe-containing active site of GolR and is probably reduced via three consecutive proton-coupled electron transfer processes. The new class of reductase, GolR, opens the chapter for the mechanistic understanding of Au(III) bioreduction.

KEYWORDS: *biogeochemical cycling of gold, microbial Au(III) reduction, Au nanoparticles, Au(III) reductase, GolR*
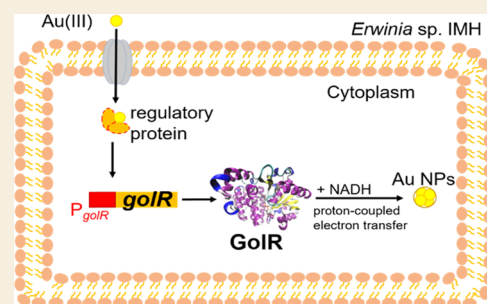
INTRODUCTION

Microorganisms are of paramount importance in the biogeochemical cycling of gold (Au) in the environment.[1−4] Au(III) is soluble and inherently toxic, whereas elemental Au is inert. As a rare metal on the earth, Au is not evenly distributed but highly enriched in mineralized zones where primary deposits (50−80 wt % of Au) and secondary grains (up to 99 wt % of Au) are formed.[2] The formation of secondary Au grains and deposits is often attributed to microbial activities.[5,6] Microorganisms, especially bacteria, reduce Au(III) to a zero-valence state as a resistance strategy[7,8] and have evolved distinct genetic, proteomic, and metabolic mechanisms to counteract Au(III) toxicity.[9,10]

Bacteria have evolved two primary pathways to detoxify Au(III), including the biochemical conversion of Au(III) to Au nanoparticles (NPs)[11,12] and the extrusion of Au(III) out of the cells.[13] In fact, Au(III) extrusion is not as widespread as other heavy metals probably due to its ready reduction to zero valence.[14] Till now, only two efflux pathways were reported. Specifically, *Salmonella enterica* has developed a Au-specific efflux system including a MerR-like transcriptional activator (GolS), a putative efflux P-type ATPase (GolT), and a metallochaperone (GolB).[13,15] In addition, *Cupriavidus metallidurans* CH34 employs a copper-handling system encoded by *copABCD* for pumping Au(III) into the periplasmic space.[16]

Microbial reduction of Au(III) to lower toxic Au NPs often occurs in the cytoplasmic and extracellular spaces. Extracellular polymeric substances (EPS) are involved in extra-cellular Au(III) reduction in numerous bacterial strains.[11,17] Meanwhile, strains of *Delftia acidovorans* secrete metallophore delftibactin to reduce Au(III) to Au NPs, which is regulated by *delG* as a response to Au(III) threat.[8] In addition, the formation of Au NPs was often observed in the cytoplasm,[18] and Au usually bonds with amino acids.[19−21] We thus propose that a reductase mediates Au(III) reduction as a microbial detoxification mechanism. As a justification of our surmise, nicotinamide adenine dinucleotide-dependent enzymes were found to catalyze Au(III) reduction via a well-established electron-donating regeneration system.[22] Notably, copper resistance genes in *Cupriavidus metallidurans* CH34 were initially assumed to regulate the Au(III) bioreduction.[7] However, the gene knockout results in the following study proved that these copper resistance genes are involved in Au(III) resistance but are not specific for Au(III) reduction.[16]
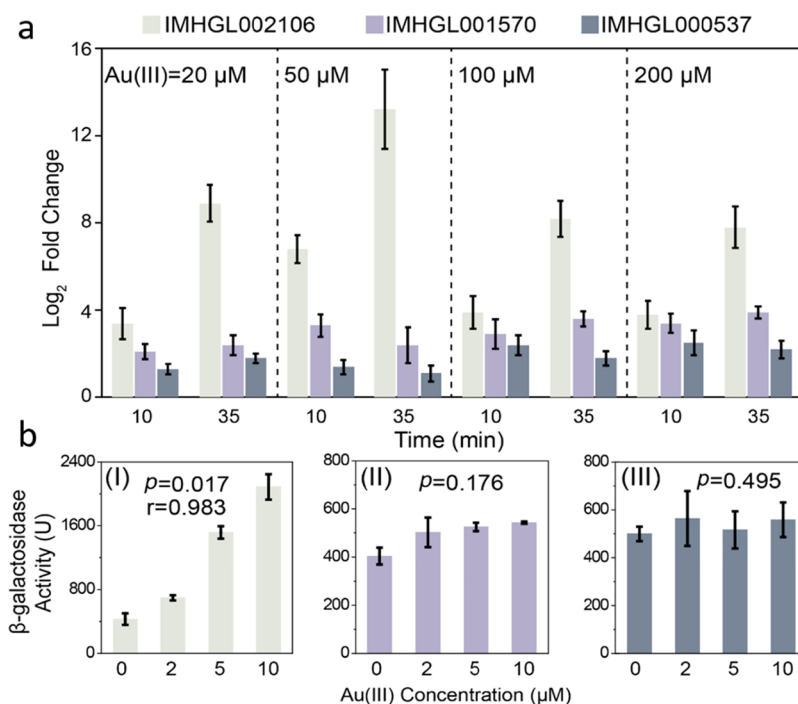
Figure 1. Q-RT PCR analysis of changes in the expression of three representative genes in response to different Au(III) concentrations at 10 and 35 min induction. (a) Gene expression was normalized to that of 16S rRNA gene. (b) β-Galactosidase activity driven by IMHGL002106, IMHGL001570, and IMHGL000537 promoters at different Au(III) concentrations. Data are shown as the mean of three replicates, with errors bars corresponding to one standard deviation.

Till now, the microbial Au(III) reductase has not yet been identified.

The motivation of this study is to discover the reductase and electron transfer pathway involved in cytoplasmic Au(III) reduction. Our previous study found that *Erwinia* sp. IMH, a multiple metal resistance bacterium isolated from Au ores,[23] is capable of reducing Au(III) to Au NPs both extra- and intracellularly.[11] Here, we describe the identification and characterization of a novel NADH-dependent Au(III) reductase referred to as GolR from *Erwinia* sp. IMH. We investigated GolR activity in vivo and in vitro and explored the interaction of Au(III) with GolR by molecular dynamic (MD) simulations and density functional theory (DFT) calculations. GolR represents a previously unrecognized class of enzymes involved in cytoplasmic Au(III) reduction as a detoxification strategy.

RESULTS AND DISCUSSION

### Identification of a Candidate Au(III) Reductase

Our previous work showed that genes regulated Au NP formation.[11] To identify genes that respond positively to Au(III) challenge and possibly mediate Au(III) reduction in IMH, we analyzed transcriptome results and focused on three oxidoreductases, which have a potential functional role in Au(III) reduction. The most strongly upregulated oxidoreductase was a dehydrogenase (IMHGL002106) (Figure S1), with a 5.2-fold up-regulation after 35 min of Au(III) exposure. The next two most up-regulated oxidoreductase genes were annotated as glutathione-independent formaldehyde dehydrogenase FdhA (IMHGL001570)[24] up to 4.2-fold up-regulation after 35 min and 7-cyano-7-deazaguanine reductase QueF (IMHGL000537)[25] up to 2.7-fold up-regulation after 35 min (Figure S1).

To verify the positive transcriptional response of these three oxidoreductase genes to the Au(III) challenge, the response of three genes to different doses of Au(III) after 10 and 35 min exposure was analyzed by real-time quantitative polymerase chain reaction (RT-qPCR). In agreement with the global transcription analysis, IMHGL002106 was up-regulated most strongly among the three genes analyzed, and its expression was constantly increased with time regardless of the initial Au(III) concentration (Figure 1a). Meanwhile, IMHGL002106 transcription was increased with increasing Au(III) concentrations from 20 to 50 μM, but no concentration dependency was found at 100 and 200 μM Au(III) (Figure 1a). This is probably because the growth of IMH was greatly inhibited at such high Au(III) concentrations.[11] Compared with IMHGL002106, IMHGL000537 and IMHGL001570 showed no dependency on time and Au(III) concentration.

To explain the different responses of IMHGL002106, IMHGL000537, and IMHGL001570 to the Au(III) challenge, the activity of their promoters was examined in *E. coli* DH 5a challenged with different Au(III) concentrations. Interestingly, IMHGL002106::*lacZ* expression was linearly correlated (p = 0.017) with the Au(III) concentration, whereas IM-HGL001570::*lacZ* and IMHGL000537::*lacZ* expression exhibited no dependence on Au(III) concentration (p > 0.1, Figure 1b). This observation indicates that the expression of IMHGL002106 but not that of IMHGL001570 and IMHGL000537 is directly induced by Au(III) acting on the gene promoter. These results suggest that IMHGL002106 may be an ideal candidate gold reductase, denoted as GolR. Thus, our subsequent efforts were focused on *golR*.

Au(III) Reduction and Resistance Mediated by GolR

To explore the relationship between GolR and Au(III) reduction in *Erwinia* sp. IMH, a mutant strain (Δ*golR*) with nonpolar deletion of *golR* and a complemented strain (Δ*golR*-C) were constructed. The diagnostic PCR was used to verify that the deletion and complementation experiments were successful (Figure S2). Then, the ability of the strains to reduce Au(III) was tested by UV−vis and transmission electron microscopy (TEM) analysis. The results showed that the wild-type IMH strain changed the color of the clear Au(III) solution to intense claret after overnight incubation, with a strong surface plasmon resonance (SPR) of Au NPs at approximately 540 nm (Figure 2a,b).[26] Consistently, TEM
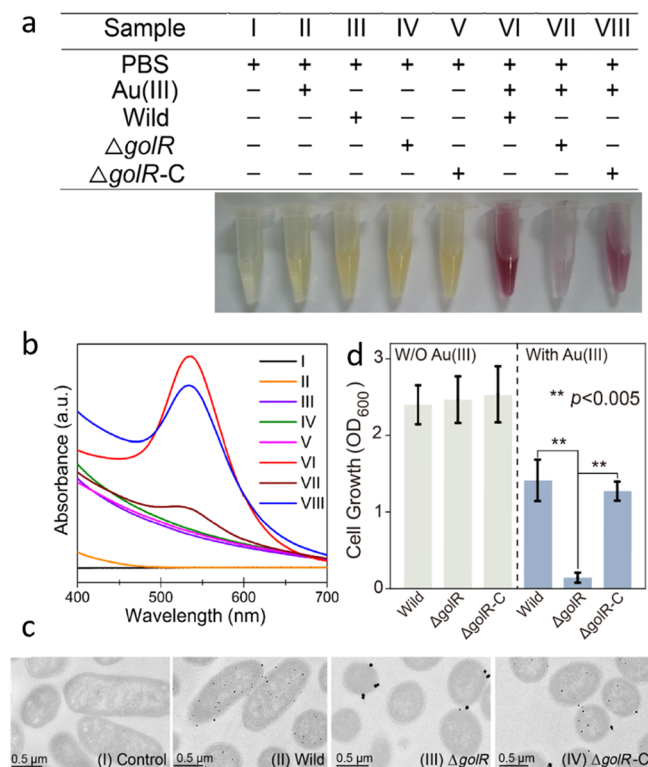
Figure 2. (a) Biosynthesis and (b) UV/vis spectra of Au NPs in different conditions. (I) PBS only; (II) PBS + 2 mM Au(III); (III) PBS + IMH; (IV) PBS + Δ*golR*; (V) PBS + Δ*golR*-C; (VI) PBS + IMH + 2 mM Au(III); (VII) PBS + Δ*golR* + 2 mM Au(III); and (VIII) PBS + Δ*golR*-C + 2 mM Au(III). (c) HR-TEM images of nanoparticles formed in the wild strain IMH, the mutant Δ*golR*, and the complementary strain Δ*golR*-C. Sensitivity assays of the wild strain IMH, the mutant strain Δ*golR*, and the complementary strain Δ*golR*-C in the absence and presence of toxic Au(III). The (d) results are shown as the mean of three replicates with errors bars corresponding to one standard deviation (two-tailed Student's *t* test).

with energy-dispersive spectrometry confirmed the presence of Au NPs, and a lattice fringe spacing of 0.224 nm was assigned to (111) of Au NPs (Figure S3).[27] By contrast, the color of Δ*golR* culture turned pale pink with a much suppressed UV−vis absorption peak at 540 nm, suggesting the absence of Au NPs. The complemented strain (Δ*golR*-C) turned the culture color to claret, with a partial but marked recovery of the 540 nm absorption peak, indicative of biogenic Au NP formation (Figure 2a,b). This indicates that *golR* plays a key role in the reduction of Au(III) to Au NPs.

To locate the position of Au NP formation, a 70 nm thick thin slice of strains was analyzed using TEM. The results revealed that Au NPs were present in the cytoplasm of wild-type IMH but not that of Δ*golR* cells or wild-type cells in the absence of Au(III) (Figure 2c). When *golR* deletion was complemented in Δ*golR*-C strain, Au NPs were detected in the cytoplasm (Figure 2c). These observations strongly indicate that Au(III) reduction mediated by GolR occurred in the cytoplasm of IMH.

To assess the importance of GolR in the Au(III) detoxification network, the growth of the three IMH strains (wild-type, Δ*golR*, and Δ*golR*-C) was monitored in the presence of 50 μM Au(III). Figure 2d shows that *golR* deletion significantly ($p < 0.005$) increased the sensitivity to Au(III) toxicity, and the complementation of *golR* rescued its resistance to Au(III) to the same level as the wild type ($p < 0.005$). These results indicate that GolR was employed to protect IMH from toxic soluble Au. It is the active strategy of IMH to employ cytoplasmic GolR to detoxify Au(III). In fact, IMH has developed multiple pathways to resist Au(III) threat. Upon sorption of Au(III) to cell surfaces, Au(III) was readily reduced to Au NPs by EPS.[11] When Au(III) sneaked the first protective barrier into the cytoplasm, intracellular reductants such as GSH resumed the responsibility for detoxification. Actually, GSH is abundant in bacteria and able to resist metal toxicity as a flexible soldier.[28,29] However, in our study, GSH was consumed by Au(III)-induced reactive oxygen species, which were pronounced under Au(III) threat (Figure S4). In this case, cytoplasmic GolR was activated to catalyze Au(III) reduction. The identification of this cytoplasmic Au(III) reductase catalyzing Au(III) reduction to Au(0) can explain the presence of Au NPs in the cytoplasm of diverse bacteria (Table S1). Such an enzymatic detoxification mechanism has also been found in microbial selenate reduction to selenium NPs in *Thauera selenatis*.[29]

Au(III) Reduction by GolR In Vitro

To further explore the function of *golR*, we cloned the IMH *golR* gene, overproduced GolR in *E. coli*, and purified it in vitro (Figure S5). Then, the Au(III)-reducing activity of GolR in vitro was examined using UV−vis spectra and X-ray absorption near edge structure (XANES) analysis. In the absence of either GolR or NADH, the color of the solution did not change and there is no SPR absorption peak at 540 nm (Figure 3a). In a XANES spectrum, the white-line feature in the Au L$_{III}$-edge (11,923 eV) is associated with the transition of 2p electrons to unoccupied 5d orbitals, with a higher peak intensity corresponding to more unoccupied states of d orbitals, that is, a higher oxidation state.[30] The linear combination fitting (LCF) of XANES spectra revealed that there is about 29 or 36% Au(III) reduction by GolR or NADH alone, respectively (Figure 3b and Table S2). These results suggested that GolR or NADH alone mediates a certain degree of Au(III) reduction, but this reduction is not enough to form Au NPs.

When Au(III) was mixed with GolR and NADH, the solution turned a light claret color, with an SPR absorption peak at 540 nm, suggesting that GolR together with NADH mediated the Au(III) reduction to Au NPs (Figure 3a). In agreement with the results of UV−vis spectra, XANES analysis showed that a large degree of Au(III) reduction happened as indicative of the decreased intensity of the white-line peak, and LCF further indicated that about 67% Au(III) was reduced in 2 h (Figure 3b and Table S4). These observations confirmed
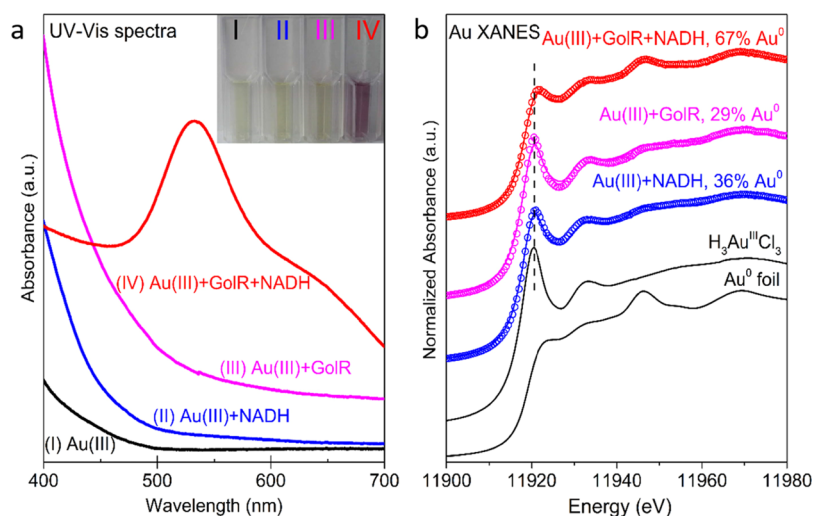
Figure 3. (a) UV−vis spectra and (b) XANES analysis of Au NPs synthesized in the treatment of Au(III) + GolR + NADH. The treatments of NADH + Au(III) and GolR + Au(III) were used as controls.

that GolR is a NADH-dependent Au(III) reductase, and consistent with other NADH-dependent reductases,[31] the cofactor NADH plays an important role in GolR-catalyzed Au(III) reduction.

GolR is a Au(III) reductase and is able to reduce Cu^{2+} and Ag^+, the elements in the same group in the periodic table, as evidenced by the XPS characterization (Figure S6 and Table S3). Consistent with a previous report that Au(III) can be detoxified using a copper-specific efflux protein,[16] our results suggest that microbes adopt similar or identical pathway to resist heavy metals with similar chemical properties. GolR, however, cannot reduce other heavy metals, such as Ni^{2+}, Pd^{2+}, Zn^{2+}, and Cd^{2+} (Figure S6).

Substrate Specificity of GolR

To identify the Au(III) species in the culture medium, the distribution of Au(III) species at neutral pH was calculated. Figure S7 shows that $AuCl_2(OH)_2^-$ (42%) and $AuCl(OH)_3^-$ (47%) are dominant in a chloroauric solution. To gain insight into the molecular interactions of $AuCl_2(OH)_2^-$ or $AuCl(OH)_3^-$ and GolR, molecular docking and dynamic simulations were next performed. The docking results show that the two Au(III) species are able to remain at the vicinity of the Fe site in the GolR cavity (Figure S8). Interestingly, the MD simulations reveal that only $AuCl_2(OH)_2^-$ is able to interact with GolR, while $AuCl(OH)_3^-$ is expelled from the GolR cavity (Figure 4 and Movies S1 and S2). The instability of $AuCl(OH)_3^-$ in the cavity may be attributed to its triple hydrophilic hydroxyl groups, which render its incompatibility with the hydrophobic GolR (Figure S8). This hydrophobicity-driven selectivity by GolR was further confirmed by our MD simulations involving $AuCl_4^-$ and $Au(OH)_4^-$. The MD results clearly indicate that $AuCl_4^-$, a hydrophobic Au complex, remains in the active site, whereas $Au(OH)_4^-$, a hydrophilic complex, is ejected from the cavity after approximately 1 ns (Figure S9 and Movies S3 and S4).

In addition, we carried out in vitro Au(III) reduction under different pH conditions. The results in Figure S10 showed that Au(III) reduction by GolR is pH dependent. Specifically, a claret color, with an SPR absorption peak at 540 nm, was observed at pH 5−7. At pH 8−9, the color of the solution was light yellow and no SPR absorption peak was detected. The
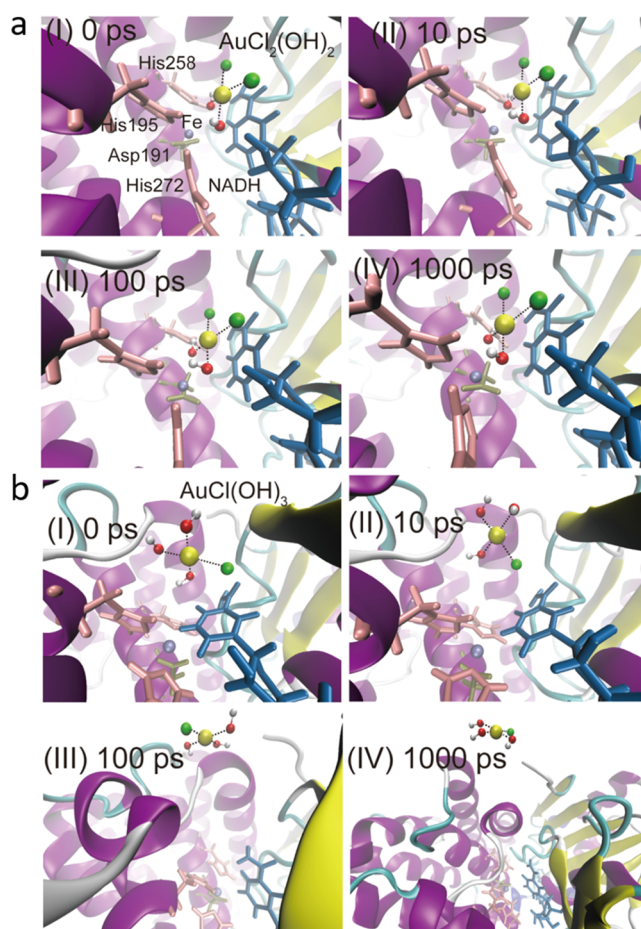
Figure 4. Snapshots of the MD simulations of (a) $AuCl_2(OH)_2^-$ and (b) $AuCl(OH)_3^-$ in the GolR cavity. Au, yellow sphere; Fe, ice-blue sphere; Cl, green sphere; O, red sphere; H, white sphere; NADH, blue sticks; His residues, pink sticks; Asp residue, tan sticks.

solution changed to brown at pH 3−4, with a weak SPR absorption peak shifted to about 560 nm. Consistent with our MD simulation results, the pH-dependent Au(III) reduction indicated that GolR may selectively react with $AuCl_2(OH)_2^-$ and $AuCl_4^-$, rather than $AuCl(OH)_3^-$ and $Au(OH)_4^-$.
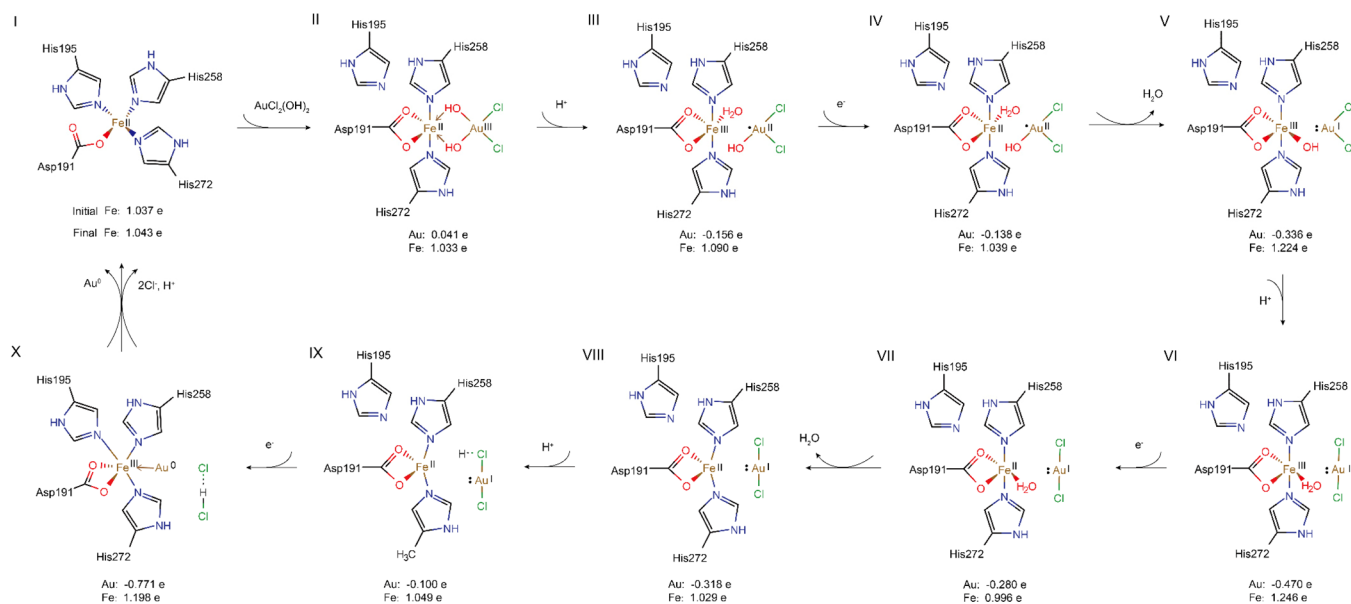
Figure 5. Calculated pathways for Au(III) reduction by GolR. The Mulliken charges of Fe and Au atoms are shown under each structure.

The selectivity of GolR toward $AuCl_2(OH)_2^-$ leads to a stable Au(III) complex on the Fe site in the cavity, as shown in Figure S11. Specifically, the bond between Fe and N on the residue His195 is broken upon $AuCl_2(OH)_2^-$ attack, and Fe is coordinated with two hydroxyl groups of $AuCl_2(OH)_2^-$ with an average Fe–O distance of 2.4 Å in a six-coordinated structure (Figure S11). Meanwhile, NADH is departed from its initial position in a 1.9 Å distance from the Fe atom, and this space is replaced by $AuCl_2(OH)_2^-$, which coordinates with Fe using with two bridging OH groups, resulting in a slightly shorter Au–Fe distance (3.03 Å) than Au–NADH distances (3.20 Å). This coordination environment for $AuCl_2(OH)_2^-$ at the GolR active site lays the structural foundation for subsequent Au(III) reduction.

Pathways of Au(III) Reduction by GolR

To predict the possible pathways for the reduction of $Au^{III}Cl_2(OH)_2^-$ to Au^0, first-principles DFT calculations were carried out. The results suggest that Au(III) reduction may be realized in three consecutive proton-coupled electron transfer (PCET) steps with an exothermic reaction in each step (Figures 5 and S12). To quantify the electron transfer, we calculated the Mulliken charges of Fe and Au atoms where more positive values represent fewer electrons. Specifically, in the first step, $Au^{III}Cl_2(OH)_2^-$ donates one OH group to react with a H^+ to form H_2O at the Fe site, and $Au^{III}Cl_2OH$ then accepts an electron from NADH to become $Au^{II}Cl_2OH^-$ (Figure 5II to III). The Mulliken charge of Au is increased from 0.041 to −0.156 e, and that of Fe is reduced from 1.033 to 1.090 e, indicating the electron transfer from Fe to Au atoms. The oxidized Fe^{III} is subsequently reduced to Fe^{II} by electrons provided by NADH, as evidenced by the increase in its Mulliken charge from 1.090 to 1.039 e (Figure 5IV). With the release of H_2O away from the Fe site, the OH group of $Au^{II}Cl_2OH^-$ is coordinated to Fe, resulting in the formation of a five-coordinated Fe^{III} complex and $Au^ICl_2^-$ (Figure 5V). Correspondingly, the Mulliken charge is decreased from 1.039 to 1.224 e on Fe and is increased from −0.138 to −0.336 e on Au. The resulting Au intermediate, $Au^ICl_2^-$, exhibits a Cl–Au–Cl angle of 103.4° with a Au–Fe distance of 2.64 Å.

Similarly, in the second PCET step, the OH group on the Fe^{III} complex reacts with a H^+ to from H_2O at the Fe site (Figure 5VI), and Fe^{III} is reduced to Fe^{II} by the electrons from NADH (Figure 5VII). Then, the formed H_2O is departed from the Fe site, leaving the linear $Au^ICl_2^-$ at a Au–Fe distance of 3.07 Å (Figure 5VIII). Consequently, the Mulliken charges of Fe and Au are changed to 1.029 and −0.318 e, respectively.

Finally, $Au^ICl_2^-$ is reduced to Au^0 in the third PCET step. $Au^ICl_2^-$ first uptakes a H^+ from NADH, resulting in a H–Cl bond with an atomic distance of 1.72 Å (Figure 5IX). Then, HAu^ICl_2 is reduced to Au^0, which stays at a Au–Fe distance of 2.54 Å, leaving the two Cl atoms in an association with a H^+ at an average H–Cl distance of 1.73 Å (Figure 5X). Similarly, the Mulliken charge analysis indicates the electron transfer from Fe to Au atoms. At the end, the Fe^{II} active site is regenerated by releasing Au^0, H, and Cl atoms (Figure 5X to I), and the Mulliken charge of Fe after regeneration (1.043 e) is comparable to that in the initial stage (1.037 e). Therefore, the Fe^{II} site at the cavity of GolR probably catalyzes the Au(III) reduction, and the resulting Au^0 aggregated to form Au NPs in the cytoplasmic space (Figure 2c).

Implications

Our multiple complementary results report a previously unknown gold reductase named GolR, which is able to reduce Au(III) to Au NPs in the cytoplasm of *Erwinia* sp. IMH. GolR may selectively capture $Au^{III}Cl_2(OH)_2^-$ rather than $Au^{III}Cl(OH)_3^-$ due to its hydrophobic nature. $Au^{III}Cl_2(OH)_2^-$ is probably reduced to Au NPs at the active Fe site in GolR by three consecutive PCET processes, involving NADH as a cofactor to provide both protons and electrons. Such a PCET process was also found in arsenate respiratory reduction mediated by ArrAB,[32] which is common for redox reactions catalyzed by oxidoreductase in bacteria. Our findings provide direct evidence that cytoplasmic Au(III) reductase is evolved and actively mediated the biogeochemical cycling of the Au element.

GolR probably contributes to a biochemically driven mineralization of Au in the environment due to its broad phylogenetic distribution (Figure S13). The organisms

containing *golR* belong to distantly related phyla within bacteria such as *Erwinia* spp.[33] and *Klebsiella pneumoniae*[34] in the phylum *Proteobacteria* and *Holdemanella biformis*[35] and *Roseburia intestinalis*[36] in the phylum *Firmicutes*. Moreover, the GolR homologue shows a high conservatism on evolution (Figure S13). For example, GolR sequences of *Erwinia* sp. IMH and *Erwinia tracheiphila* show as high as 80% similarity in amino acids. Thus, *golR* can be used as a molecular probe in metagenomics analysis to explore the possible contribution of microbial Au(III) reduction in gold mineralized zones. In addition, bio-green synthesis of Au NPs with high efficiency probably could be realized through molecular engineering based on the identification and characterization of *golR*.

■ MATERIALS AND METHODS

Strains, Plasmids, and Culture Conditions

Bacterial strains of *Erwinia*, *E. coli*, and plasmids used or constructed in this study are listed in Table S4. *Erwinia* and *E. coli* strains were cultured at 30 or 37 °C in the Luria-Bertani (LB) medium, respectively. When needed for the culture of *E. coli* WM3064, diaminopimelic acid (DAP, 30 mM) was added. When needed for the culture of strains containing plasmid, the corresponding antibiotics were added.

Quantitative RT-PCR Analysis

To verify the transcriptome data and identify the transcriptional level of the Au-induced genes, *Erwinia* sp. IMH was cultivated and challenged with different Au(III) concentrations. Then, RNA was isolated and cDNA was synthesized as described in the Supporting Information (SI). RT-qPCR was performed according to the SYBR Premix ExTaq II Reagent Kit (TaKaRa, Japan) protocol,[37] and three technical and biological replicates were established for each reaction. Primers used for the reactions are listed in Table S5. Gene expression was normalized based on ΔC_T calculations,[38] using an iQ5 Real-Time PCR detection system (Bio-Rad, USA). The expression of the 16S rRNA gene was used as a reference in the calculations.

Construction of the Δ*golR* Mutant and Complementation of IMH

To determine whether *golR* was required for intracellular Au(III) reduction, a mutant with in-frame deletion of *golR* (Δ*golR* strain) was constructed. The primers used for the construction of the deletion are listed in Table S5. The PCR product was cloned into pSMV10 double-digested with *Sep*I-*Bam*HI, yielding pΔ*golR*, which was then transformed into strain IMH via conjugation with *E. coli* WM3064. Single-crossover mutants were screened on LB agar containing 10% sucrose, and kanamycin-sensitive colonies were screened and verified by PCR using primers GolR-up-F and GolR-down-R (Table S5).

For Δ*golR* complementation, the complete *golR* coding region with a gene promoter was PCR cloned as a *Kpn*I and *Hind*III fragment into pUC18 and then transferred to Δ*golR* strain by conjugation via *E. coli* WM3064. The resultant strain was named Δ*golR*-C. The complemented strain was further verified by PCR using primers GolR-F and GolR-R (Table S5).

Promotor Activity

To understand the promotor activities in the presence of Au(III), promoters of IMHGL002106, IMHGL000537, and IMHGL001570 genes were fused to the *lacZ* gene of ppR9TT, and β-galactosidase assays were analyzed. Three promotors were PCR-cloned as *Kpn*I-*Sma*I fragments into *lacZ* reporter plasmid pPR9TT, respectively. The resulting plasmids were transformed into *E. coli* DH5α, yielding *E. coli* DH5α/pPR9TT-P2106, *E. coli* DH5α/pPR9TT-P0537, and *E. coli* DH5α/pPR9TT-P1570. For β-galactosidase activity assays, three *E. coli* strains were cultured in LB for 24 h, harvested, washed three times, and resuspended in phosphate-buffered saline (PBS) buffer (pH 7.0) with different Au(III) concentrations at 30 °C for 35 min. Then, the cells were harvested, and β-galactosidase activity was

measured according to the method described by Miller.[39] All of the experiments were performed in triplicate.

Au(III) Reduction and Sensitivity Assays

To investigate the relation between *golR* and Au(III) reduction, Au(III) reduction and sensitivity assays of wild-type IMH, mutant Δ*golR*, and complementary Δ*golR*-C were carried out. For Au(III) reduction, IMH, Δ*golR*, and Δ*golR*-C were cultured in LB for 24 h, harvested, washed three times, and resuspended in PBS buffer (pH 7.0) with 2 mM Au(III) at 30 °C on a rotary shaker (160 rpm) overnight. Then, each sample was taken for detecting the SPR of Au NPs using UV−vis spectroscopy (UV-2550 Shimadzu) at 540 nm. At the same time, the cells were harvested, washed with PBS buffer (pH 7.0) three times, and fixed with 0.15% glutaraldehyde in phosphate buffer (pH 7.0) at 4 °C for overnight. The fixed cells were dehydrated with graded ethanol (75−100%) series and embedded in resin. The samples were then thin sectioned (70 nm) in ultramicrotome using a diamond knife and collected on a carbon-coated copper grid. Our previous work showed that the particle formed in our condition was identified as Au NPs. Localization of Au NPs was observed from high-resolution TEM (Tecnai G2 F20, FEI).

For Au(III) sensitivity assays, overnight cultures of IMH, Δ*golR*, and Δ*golR*-C were inoculated into 100 mL of fresh LB medium containing 50 μM Au(III) and incubated at 30 °C on a rotary shaker (160 rpm) for 72 h, and control experiments without Au(III) were also performed. Cell growth was monitored at OD_{600} using a spectrophotometer (DR2800, HACH, USA). The experiments were performed in triplicate.

In Vitro Au(III) Reduction by GolR

To measure the Au(III) reduction activity of GolR in vitro, GolR was overexpressed and purified as described in the SI. The coenzyme requirement was determined first, and no GolR activity was detected in the absence of NADH, whereas Au(III) was actively reduced when NADH was added. For Au(III) reduction by GolR in vitro, 1 mM GolR and 1 mM NADH were incubated with 2 mM Au(III) in Tris−HCl (pH 7.0) at 30 °C in quartz cuvettes for 2 h. NADH or GolR alone incubated with 2 mM Au(III) was used as the control. The formation of Au NPs was monitored by using a UV−vis spectrometer (UV-2550 Shimadzu) at 540 nm. All experiments were carried out in triplicate. Then, the samples were centrifuged at 6000 × g (Thermo Scientific, USA) for 10 min and washed three times with PBS (pH 7.0). These washed samples were flash cooled in liquid nitrogen and freeze-dried overnight. Then, the XANES spectra at the Au L_{III}-edge were collected at beamline 14 W1 at the Shanghai Synchrotron Radiation Facility, China. An energy range of −200 to 650 eV from the L_{III}-edge of Au (11,919 eV) was used for spectrum acquisition. The spectra were analyzed using a LCF in the Athena program.[40] The data processing and fitting approach followed our previous report.[11]

Molecular Docking and Dynamic Simulations

To calculate the molecular interactions of Au(III) and GolR, molecular docking and dynamic simulations were carried out. First, Au complexes, including $AuCl_2(OH)_2^-$, $AuCl(OH)_3^-$, $AuCl_4^-$, and $Au(OH)_4^-$, were geometry optimized in the Gaussian 09 program with B3LYP hybrid DFT using the 6-31G* basis set for O, H, and Cl and the LanL2DZ basis set for Au. Then, molecular docking of Au complexes with GolR was performed by the homology model and CDOCKER protocol in Discovery Studio Software (DS, Accelrys, San Diego, CA, United States). Finally, the MD simulations were conducted in Amber software with Amber Tools 18, and MCPB.py has been performed to build force fields for the simulation of metal complexes of $AuCl_2(OH)_2^-$ and $AuCl(OH)_3^-$. The details are described in the SI.

DFT Calculations for Au(III) Reduction

To predict the possible pathways for the Au(III) reduction by GolR, DFT calculations were carried out. The stable structure after MD runs was extracted by selecting the $AuCl_2(OH)_2^-$ molecule and residues that are in the 5.0 Å range. It is acknowledged that the NADH cofactor is the electron donor and a dehydrogenase. Thus, the extra

electrons and protons were added in the system to replace NADH to compensate computational cost. The reduced Au(III) structures were optimized in the Gaussian 09 program using the 6-31G* basis set for C, H, O, N, Cl, and Fe and the LanL2DZ basis set for Au. The reduction process was examined, and the reaction energy was calculated.

■ ASSOCIATED CONTENT

Ⓢ Supporting Information

The Supporting Information is available free of charge at https://pubs.acs.org/doi/10.1021/jacsau.2c00170.

$AuCl_2(OH)_2^-$ interaction with GolR (Movie S1) (AVI)

$AuCl(OH)_3^-$ expelled from the GolR cavity (Movie S2) (AVI)

$AuCl_4^-$, a hydrophobic Au complex, remaining in the active site (Movie S3) (AVI)

$Au(OH)_4^-$, a hydrophilic complex, ejected from the cavity after approximately 1 ns (Movie S4) (AVI)

Details of cell growth, RNA isolation, cDNA synthesis, GolR purification, phylogenetic analysis, electrophoretic mobility shift assays, molecular docking, molecular dynamic simulations, and additional figures and tables (PDF)

■ AUTHOR INFORMATION

Corresponding Author

Chuanyong Jing − *State Key Laboratory of Environmental Chemistry and Ecotoxicology, Research Center for Eco-Environmental Sciences, Chinese Academy of Sciences, Beijing 100085, China; School of Environmental Science and Engineering, Shandong University, Qingdao 266237, China;* ⓞ orcid.org/0000-0002-4475-7027; Phone: +86 10 6284 9523; Email: cyjing@rcees.ac.cn

Authors

Liying Wang − *State Key Laboratory of Environmental Chemistry and Ecotoxicology, Research Center for Eco-Environmental Sciences, Chinese Academy of Sciences, Beijing 100085, China*

Li Yan − *State Key Laboratory of Environmental Chemistry and Ecotoxicology, Research Center for Eco-Environmental Sciences, Chinese Academy of Sciences, Beijing 100085, China*

Li Ye − *School of Environmental Science and Engineering, Shandong University, Qingdao 266237, China*

Jinfeng Chen − *Environment Research Institute, Shandong University, Qingdao 266237, China*

Yanwei Li − *Environment Research Institute, Shandong University, Qingdao 266237, China;* ⓞ orcid.org/0000-0003-4089-9789

Qingzhu Zhang − *Environment Research Institute, Shandong University, Qingdao 266237, China;* ⓞ orcid.org/0000-0001-7505-7755

Complete contact information is available at:
https://pubs.acs.org/10.1021/jacsau.2c00170

Author Contributions

∥L.W. and L.Y. contribute equally to this work.

Notes

The authors declare no competing financial interest.

■ REFERENCES

(1) Reith, F.; Rogers, S. L.; Mcphail, D. C.; Webb, D. Biomineralization of gold: biofilms on bacterioform gold. *Science* **2006**, *313*, 233−236.

(2) Reith, F.; Lengke, M. F.; Falconer, D.; Craw, D.; Southam, G. The geomicrobiology of gold. *ISME J.* **2007**, *1*, 567−584.

(3) Reith, F.; Mcphail, D. C. Effect of resident microbiota on the solubilization of gold in soil from the Tomakin Park Gold Mine, New South Wales, Australia. *Geochim. Cosmochim. Acta* **2006**, *70*, 1421−1438.

(4) Reith, F.; Brugger, J. L.; Zammit, C.; Nies, D.; Southam, G. Geobiological cycling of gold: from fundamental process understanding to exploration solutions. *Minerals* **2013**, *3*, 367−394.

(5) Fairbrother, L.; Etschmann, B.; Brugger, J.; Shapter, J.; Southam, G.; Reith, F. Biomineralization of gold in biofilms of *Cupriavidus metallidurans*. *Environ. Sci. Technol.* **2013**, *47*, 2628−2635.

(6) Reith, F.; Fairbrother, L.; Nolze, G.; Wilhelmi, O.; Clode, P. L.; Gregg, A.; Parsons, J. E.; Wakelin, S. A.; Pring, A.; Hough, R. Nanoparticle factories: biofilms hold the key to gold dispersion and nugget formation. *Geology* **2010**, *38*, 843−846.

(7) Reith, F.; Etschmann, B.; Grosse, C.; Moors, H.; Benotmane, M. A.; Monsieurs, P.; Grass, G.; Doonan, C.; Vogt, S.; Lai, B.; Martinez-Criado, G.; George, G. N.; Nies, D. H.; Mergeay, M.; Pring, A.; Southam, G.; Brugger, J. Mechanisms of gold biomineralization in the bacterium *Cupriavidus metallidurans*. *Proc. Natl. Acad. Sci. U. S. A.* **2009**, *106*, 17757−17762.

(8) Johnston, C. W.; Wyatt, M. A.; Li, X.; Ibrahim, A.; Shuster, J.; Southam, G.; Magarvey, N. A. Gold biomineralization by a metallophore from a gold-associated microbe. *Nat. Chem. Biol.* **2013**, *9*, 241−243.

(9) Mergeay, M.; Monchy, S.; Vallaeys, T.; Auquier, V.; Benotmane, A.; Bertin, P.; Taghavi, S.; Dunn, J.; van der Lelie, D.; Wattiez, R. *Ralstonia metallidurans*, a bacterium specifically adapted to toxic metals: towards a catalogue of metal-responsive genes. *FEMS Microbiol. Rev.* **2003**, *27*, 385−410.

(10) Nies, D. H. Microbial heavy-metal resistance. *Appl. Microbiol. Biotechnol.* **1999**, *51*, 730−750.

(11) Liu, W.; Wang, L.; Wang, J.; Du, J.; Jing, C. New insights into microbial-mediated synthesis of Au@biolayer nanoparticles. *Environ. Sci.: Nano* **2018**, *5*, 1757−1763.

(12) Konishi, Y.; Tsukiyama, T.; Tachimi, T.; Saitoh, N.; Nomura, T.; Nagamine, S. Microbial deposition of gold nanoparticles by the metal-reducing bacterium *Shewanella algae*. *Electrochim. Acta* **2007**, *53*, 186−192.

(13) Pontel, L. B.; Audero, M. E. P.; Espariz, M.; Checa, S. K.; Soncini, F. C. GolS controls the response to gold by the hierarchical induction of *Salmonella*-specific genes that include a CBA efflux-coding operon. *Mol. Microbiol.* **2007**, *66*, 814−825.

(14) Usher, A.; McPhail, D. C.; Brugger, J. A spectrophotometric study of aqueous Au(III) halide-hydroxide complexes at 25−80 degrees C. *Geochim. Cosmochim. Acta* **2009**, *73*, 3359−3380.

(15) Checa, S. K.; Espariz, M.; Perez Audero, M. E.; Botta, P. E.; Spinelli, S. V.; Soncini, F. C. Bacterial sensing of and resistance to gold salts. *Mol. Microbiol.* **2007**, *63*, 1307−1318.

(16) Wiesemann, N.; Mohr, J.; Grosse, C.; Herzberg, M.; Hause, G.; Reith, F.; Nies, D. H. Influence of copper resistance determinants on gold transformation by *Cupriavidus metallidurans* strain CH34. *J. Bacteriol.* **2013**, *195*, 2298−2308.

(17) Kang, F.; Qu, X.; Alvarez, P. J. J.; Zhu, D. Extracellular saccharide-mediated reduction of Au^{3+} to gold nanoparticles: New insights for heavy metals biomineralization on microbial surfaces. *Environ. Sci. Technol.* **2017**, *51*, 2776−2785.

(18) Lloyd, J. R. Microbial reduction of metals and radionuclides. *FEMS Microbiol.* **2010**, *27*, 411−425.

(19) Kalishwaralal, K.; Deepak, V.; Pandian, S. R. K.; Kottaisamy, M.; BarathManiKanth, S.; Kartikeyan, B.; Gurunathan, S. Biosynthesis of silver and gold nanoparticles using *Brevibacterium casei*. *Colloids Surf., B* **2010**, *77*, 257−262.

(20) He, S.; Guo, Z.; Zhang, Y.; Zhang, S.; Wang, J.; Gu, N. Biosynthesis of gold nanoparticles using the bacteria *Rhodopseudomonas capsulata*. *Mater. Lett.* **2007**, *61*, 3984−3987.

(21) Zou, T.; Lum, C. T.; Chui, S. S. Y.; Che, C. M. Gold(III) complexes containing N-heterocyclic carbene ligands: Thiol :switch-on" fluorescent probes and anti-cancer agents. *Angew. Chem., Int. Ed. Engl.* **2013**, *52*, 2930−2933.

(22) Niide, T.; Goto, M.; Kamiya, N. Biocatalytic synthesis of gold nanoparticles with cofactor regeneration in recombinant *Escherichia coli* cells. *Chem. Commun.* **2011**, *47*, 7350−7352.

(23) Li, M.; Tian, H.; Wang, L.; Duan, J. Bacterial diversity in Linglong gold mine, China. *Geomicrobiol. J.* **2017**, *34*, 267−273.

(24) Ito, K.; Takahashi, M.; Yoshimoto, T.; Tsuru, D. Cloning and high-level expression of the glutathione-independent formaldehyde dehydrogenase gene from *Pseudomonas putida*. *J. Bacteriol.* **1994**, *176*, 2483−2491.

(25) Swairjo, M. A.; Reddy, R. R.; Lee, B.; Van Lanen, S. G.; Brown, S.; de Crecy-Lagard, V.; Iwata-Reuyl, D.; Schimmel, P. Crystallization and preliminary X-ray characterization of the nitrile reductase QueF: A queuosine-biosynthesis enzyme. *Acta Crystallogr., Sect. F: Struct. Biol. Cryst. Commun.* **2005**, *61*, 945−948.

(26) Das, S. K.; Dickinson, C.; Lafir, F.; Brougham, D. F.; Marsili, E. Synthesis, characterization and catalytic activity of gold nanoparticles biosynthesized with *Rhizopus oryzae* protein extract. *Green Chem.* **2012**, *14*, 1322−1334.

(27) Boccuzzi, F.; Cerrato, G.; Pinna, F.; Strukul, G. FTIR, UV−Vis, and HRTEM study of Au/ZrO₂ catalyst: reduced reactivity in the CO−O₂ reaction of electron-deficient gold sites present on the used samples. *J. Phys. Chem. B* **1998**, *102*, 5733−5736.

(28) Kessi, J.; Hanselmann, K. W. Similarities between the abiotic reduction of selenite with glutathione and the dissimilatory reaction mediated by *Rhodospirillum rubrum* and *Escherichia coli*. *J. Biol. Chem.* **2004**, *279*, 50662−50669.

(29) Debieux, C. M.; Dridge, E. J.; Mueller, C. M.; Splatt, P.; Paszkiewicz, K.; Knight, I.; Florance, H.; Love, J.; Titball, R. W.; Lewis, R. J.; Richardson, D. J.; Butler, C. S. A bacterial process for selenium nanosphere assembly. *Proc. Natl. Acad. Sci. U. S. A.* **2011**, *108*, 13480−13485.

(30) Zhang, P.; Sham, T. K. X-ray studies of the structure and electronic behavior of alkanethiolate-capped gold nanoparticles: The interplay of size and surface effects. *Phys. Rev. Lett.* **2003**, *90*, No. 245502.

(31) Park, C. H.; Keyhan, M.; Wielinga, B.; Fendorf, S.; Matin, A. Purification to homogeneity and characterization of a novel *Pseudomonas putida* chromate reductase. *Appl. Environ. Microbiol.* **2000**, *66*, 1788−1795.

(32) Glasser, N. R.; Oyala, P. H.; Osborne, T. H.; Santini, J. M.; Newman, D. K. Structural and mechanistic analysis of the arsenate respiratory reductase provides insight into environmental arsenic transformations. *Proc. Natl. Acad. Sci. U. S. A.* **2018**, *115*, E8614−E8623.

(33) Wang, L.; Wang, J.; Jing, C. Comparative genomic analysis reveals organization, function and evolution of *ars* genes in *Pantoea* spp. *Front. Microbiol.* **2017**, *8*, No. e1000859.

(34) Brisse, S.; Grimont, F.; Grimont, P. A. D. In *The Prokaryotes: The Genus Klebsiella*, Dworkin, M., Falkow, S., Rosenberg, E., Schleifer, K. H., Stackebrandt, E., Eds.; Springer, 2006.

(35) De Maesschalck, C.; Van Immerseel, F.; Eeckhaut, V.; De Baere, S.; Cnockaert, M.; Croubels, S.; Haesebrouck, F.; Ducatelle, R.; Vandamme, P. *Faecalicoccus acidiformans* gen. nov., sp. nov., isolated from the chicken caecum, and reclassification of *Streptococcus pleomorphus* (Barnes et al. 1977), *Eubacterium biforme* (Eggerth 1935) and *Eubacterium cylindroides* (Cato et al. 1974) as *Faecalicoccus pleomorphus* comb. nov., *Holdemanella biformis* gen. nov., comb. nov and *Faecalitalea cylindroides* gen. nov., comb. nov., respectively, within the family *Erysipelotrichaceae*. *Int. J. Syst. Evol. Microbiol.* **2014**, *64*, 3877−3884.

(36) Duncan, S. H.; Hold, G. L.; Barcenilla, A.; Stewart, C. S.; Flint, H. J. *Roseburia intestinalis* sp. nov., a novel saccharolytic, butyrate-producing bacterium from human faeces. *Int. J. Syst. Evol. Microbiol.* **2002**, *52*, 1615−1620.

(37) Wyatt, M. F.; Stein, B. K.; Brenton, A. G. Characterization of various analytes using matrix-assisted laser desorption/ionization time-of-flight mass spectrometry and 2-(2E)-3-(4-tert-butylphenyl).2-methylprop-2-enylidene malononitrile matrix. *Anal. Chem.* **2006**, *78*, 199−206.

(38) Livak, K. J.; Schmittgen, T. D. Analysis of relative gene expression data using real-time quantitative PCR and the $2^{-\Delta\Delta C_T}$ method. *Methods* **2001**, *25*, 402−408.

(39) Miller; Jeffrey, H. *Experiments in molecular genetics*; Cold Spring Harbor Laboratory, 1972.

(40) Ravel, B.; Newville, M. ATHENA, ARTEMIS, HEPHAESTUS: Data analysis for X-ray absorption spectroscopy using IFEFFIT. *J. Synchrotron Radiat.* **2010**, *12*, 537−541.

■ NOTE ADDED AFTER ASAP PUBLICATION

This paper was published on May 19, 2022. Minus signs were added to the formulas for negatively charged compounds throughout the text, and the corrected version was reposted on May 25, 2022.